Electromagnetic response of nanosphere pairs: Collective plasmon resonances, enhanced fields, and laser-induced forces

Ping Chu* and D. L. Mills†
Department of Physics and Astronomy, University of California, Irvine, California 92697, USA
(Received 5 November 2007; published 18 January 2008)

We present theoretical studies of the electromagnetic response of metallic nanosphere pairs, with emphasis on the role of their collective plasmon resonances in enhancing electromagnetic fields in their near vicinity, and also in enhancing laser-induced forces between the particles. We emphasize effects encountered when the two particles have dissimilar radii or are fabricated from dissimilar materials. The calculations explore the response of the particles to electric fields polarized parallel and perpendicular to the line between their centers. We find, compared to two identical spheres, that on resonance, both the maximum enhancement in the electric fields and the laser-induced force are increased when the radii differ. Also, there is a breakdown of the selection rule associated with reflection symmetry through the plane which passes through the midpoint of the line between centers. A result is that all collective modes are dipole active when the spheres are dissimilar, for electric fields both parallel to and perpendicular to the line between the sphere centers. Our analysis exploits the electrostatic approximation appropriate to nanoscale objects but is exact within this framework without resort to a dipole approximation.

DOI: 10.1103/PhysRevB.77.045416 PACS number(s): 78.67.−n, 73.22.Lp, 78.20.Bh

I. INTRODUCTION

For a very long time, the study of the dynamic response of ever smaller entities has been an active area of experimental and theoretical research. One encounters new physics as the linear dimensions of objects studied approach nanoscales or even atomic dimensions, and new applications of such very small scale structures can have a dramatic impact on technology.

Linear and nonlinear optical spectroscopies are actively exploited to study very small entities. Over 30 years ago, the discovery of surface enhanced Raman scattering,[1] (SERS) opened up the spectroscopy of submonolayer quantities of molecules in the electrochemical environment. Rather soon after the discovery of these dramatic enhancements of the Raman cross sections, it became apparent that a crucial issue is the local enhancement of electromagnetic fields through coupling of both the incident and scattered photon either to localized plasmons associated with large structures on the surface or to surface polaritons on samples that may be viewed as somewhat roughened.[2] It also became apparent[3,4] that the electromagnetic enhancement effects were supplemented by substantial increases in the Raman cross section of molecules adsorbed on metal surfaces, through charge transfer excitations absent when the molecule is in the gas or liquid phase. It remains the case to the present that in a specific measurement, it is difficult to disentangle electromagnetic enhancement effects from those associated with possibly substantial increases in the Raman cross section of the adsorbed species itself. We note an elegant experiment in which it proved possible to separate these two effects in a fully unambiguous manner.[5]

In the early generation of experiments just discussed, quantitative theoretical descriptions of SERS were severely handicapped by the poorly characterized adsorption geometries in virtually all of the experiments. Strongly enhanced Raman signals were found not only on roughened metal surfaces but for molecules adsorbed on nanoscale metallic particles as well. In the latter case, laser excitation of the Mie resonance, viewed currently as a collective plasmon mode of the nanoparticle, is responsible for the field enhancements which boost the cross section. Measurements explored signals from ensembles of nanoparticles with a distribution of size and shape; so again, at the microscopic level, the nature of the adsorption sites wherein very strong enhancements were realized could be only inferred indirectly.

In recent years, there have been remarkable advances in sample preparation that take us into a regime where key elements of the sample geometry are quite well understood. For instance, signals from selected individual nanoparticles have been reported, under conditions where the nanoparticle contained only a single adsorbed molecule.[6] Measurements on ensembles suggested that there were "hot spots" associated with pairs of nanoparticles located very close to each other wherein the field enhancements were much larger than realized for isolated nanoparticles. Through use of a micromanipulator, it has proved possible to study Raman signals from selected Ag nanoparticle pairs.[7] Collective plasmon resonances of selected Au particles have been studied as well as a function of separation of the particles.[8] The collective plasmon resonances of more complex structures synthesized in the laboratory have also appeared.[9]

It should be remarked that it is not uncommon to analyze data taken on nanosphere pairs or collections of nanospheres through use of a simple model where intersphere interactions are viewed simply as dipole-dipole interactions.[8,9] Such a simple model is valid only when the intersphere separation is large compared to their diameters. When the spheres are close together, so the distance between the adjacent poles of nearby spheres is small compared to their diameter, the dipole model breaks down qualitatively, and it is necessary to utilize a theory which takes full account of the many multipoles associated with the charge motions present in individual spheres when the plasmon collective modes are ex-

cited. We note that a rather simple theoretical formulation of the collective excitations of nanosphere arrays is available, which is exact in the electrostatic limit appropriate to particles of nanoscale size.[10] With this formalism, it is quite straightforward to describe the collective plasmon excitations of diverse structures, with all multipoles included fully. The calculations reported in Ref. 10 illustrated excellent convergence, down to the point where adjacent spheres touch.

It is desirable to use various probes, such as the tip of a scanning tunneling microscope (STM), as a means of enhancing linear and nonlinear optical interactions of laser probes with a single molecule under the tip. Here, large field enhancements can be realized through excitation of the collective surface plasmons of the tip-substrate combination.[11] In a recent experiment, sub angstrom resolution has been achieved in an optical experiment which probes a single molecule under an STM tip.[12] It is evident, when signal levels obtained through use of a Ag coated tip with those present when a W tip is used, that plasmon enhancement effects similar to those explored in Ref. 11 are present. Plasmon resonances also allow single trapped nanoparticles to act as near field optical probes; enhanced fields in their near vicinity allow them to act as optical tweezers.[13]

We are thus now into a most fascinating era where one may study the collective plasmon resonances of individual nanoparticles, pairs, and other very small scale structures and one may then exploit the presence of the associated resonant response to the point where single molecules may be studied by various forms of optical spectroscopy. This motivates theoretical studies of collective plasmons in diverse nanostructures and their influence on optical interactions with them.

The present paper is devoted to theoretical studies of the optical response of pairs of metallic nanospheres, with emphasis on the case where the spheres are dissimilar, either because their radii are different or they are synthesized from different materials. The special case of a sphere in the near vicinity of a flat surface, explored in earlier work,[11] emerges as the limit when the radius of one sphere in the pair is allowed to become infinite. We explore the nature of the collective plasmon resonances of such a two-sphere system, the enhanced fields in their vicinity in response to laser excitation of the resonance modes, and also the laser-induced force between such entities. This is done within the framework of the electrostatic approximation. Through resorting to an analysis in bispherical coordinates, we present an exact solution of the problem, with all multipoles included in the description of the response. As remarked earlier, the frequently used dipole-dipole interaction picture breaks down badly when the spheres are close together. It is well known that in the electrostatic limit, the dipole-dipole interaction picture is valid only when the separation between the spheres is large compared to their radii.

We find interesting differences in the response of the two-sphere system when the spheres are dissimilar, compared to the special case of two identical spheres. In the latter case, the electrostatic potential has reflection symmetry through a plane perpendicular to the line between the sphere centers, and which passes through the midpoint of this line. The collective modes can then be classified by the symmetry of their electrostatic potential under reflection through this plane. The modes for which this potential is odd are excited by a laser field parallel to the line between the midpoints and "silent" in response to a field normal to this line. The converse is true for modes whose electrostatic potential is even under this reflection. When the spheres are dissimilar, the selection rule breaks down and all collective modes are excited by the laser field. We explore field enhancement effects for this circumstance, along with the magnitude of laser-induced forces between the entities. In an earlier paper,[14] we have presented a limited summary of calculations such as these, and length limitations prohibited a presentation of our extension of the application of bispherical coordinates to the discussion of dissimilar sphere pairs, which has been used for a number of years,[15] to the case where the spheres are identical.

The outline of this paper is as follows. In Sec. II, we present a brief summary of the formalism we have utilized. Section III presents a number of numerical results, and concluding remarks are found in Sec. IV.

II. STRUCTURE OF THE THEORY

As remarked in Sec. I, our analysis will be carried out within the framework of the electrostatic description of the electric fields in the vicinity of the nanosphere pair. This treatment will prove accurate if the radii of the two spheres are both small compared to the wavelength of the laser radiation which illuminates them. In this limit, the incident laser field may be viewed as a spatially uniform driving field, with frequency ω. Thus, the problem we address is the response of two dielectric spheres, one with radius R_1 and complex dielectric constant $\varepsilon_1(\omega)$ and the second with radius R_2 and complex dielectric constant $\varepsilon_2(\omega)$ exposed to a spatially uniform electric field. With the thought that the spheres may be embedded in a medium such as a liquid, we assume that outside the spheres the dielectric constant is ε_0 everywhere.

The problem just described may be solved exactly, without resort to approximation, through use of bispherical coordinates. In this coordinate system, a point in space is described by three coordinates (β, α, φ). The azimuthal angle φ is familiar from cylindrical coordinates. The relationship between the Cartesian coordinates (x, y, z) and the bispherical coordinates is given by

$$x = \frac{c \sin \alpha \cos \varphi}{\cosh \beta - \cos \alpha}, \tag{1a}$$

$$y = \frac{c \sin \alpha \sin \varphi}{\cosh \beta - \cos \alpha}, \tag{1b}$$

and

$$z = \frac{c \sinh \beta}{\cosh \beta - \cos \alpha}. \tag{1c}$$

What is important for our present purposes is that surfaces of constant β are spheres, with the xy plane described by $\beta = 0$. All points with $\beta > 0$ lie in the upper half space $z > 0$,

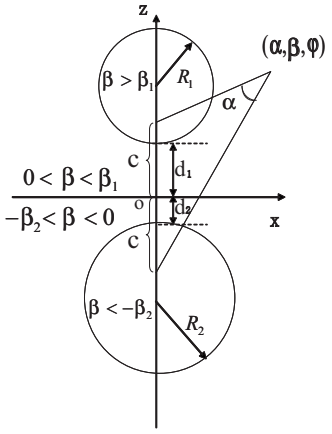

FIG. 1. The geometry considered in the present paper, as described in bispherical coordinates. See the text for a definition of the quantities illustrated in the figure.

and all points with $\beta<0$ lie in the lower half space $z<0$. If $\rho=(x^2+y^2)^{1/2}$ is the radial coordinate of a spherical coordinate system, then surfaces of constant β are given by

$$\rho^2 + (z - c\coth\beta)^2 = c^2/(\sinh\beta)^2. \tag{2}$$

The parameter c, chosen as described below, is a parameter which enters the transformation which may be chosen at one's convenience. The reader will find an introduction to bispherical coordinates in the Appendix of the paper cited first in Ref. 11. [Note that there is a typographical error in Eq. (A3) of this reference. The right hand side should read $c^2/\sin^2\alpha$.]

In Fig. 1, we show the geometry explored in the present paper, as described by bispherical coordinates. We have a sphere of radius R_1 located the distance d_1 above the xy plane and a sphere of radius R_2 located the distance d_2 below the xy plane. The distance between the south pole of the upper sphere and the north pole of the lower sphere is thus $D=d_1+d_2$. In bispherical coordinates, the equation of the upper sphere is $\beta=\beta_1$ and the equation of the lower sphere is $\beta=-\beta_2$, where we have

$$\beta_1 = \ln\left\{1 + \frac{d_1}{R_1} + \left[\left(1 + \frac{d_1}{R_1}\right)^2 - 1\right]^{1/2}\right\}, \tag{3a}$$

and

$$\beta_2 = \ln\left\{1 + \frac{d_2}{R_2} + \left[\left(1 + \frac{d_2}{R_2}\right)^2 - 1\right]^{1/2}\right\}. \tag{3b}$$

The interior of the upper sphere is the region $\beta>\beta_1$ while the interior of the lower sphere is $\beta<-\beta_2$, as illustrated in the figure. We also have the following relationships:

$$d_1 = \frac{D^2 + 2R_2D}{2(D + R_1 + R_2)}, \tag{4a}$$

$$d_2 = \frac{D^2 + 2R_1D}{2(D + R_1 + R_2)}, \tag{4b}$$

and

$$c = \sqrt{d_1(d_1 + 2R_1)} = \sqrt{d_2(d_2 + 2R_2)}. \tag{4c}$$

Notice that we also have the relation $d_2=\sqrt{R_2^2+d_1^2+2R_1d_1}-R_2$.

We shall denote the electrostatic potential by $\Phi(\beta,\alpha,\varphi)$. In bispherical coordinates, the components of the electric field are then given by

$$E_\beta = -\frac{1}{h_\beta}\frac{\partial\Phi}{\partial\beta}, \tag{5a}$$

$$E_\alpha = -\frac{1}{h_\alpha}\frac{\partial\Phi}{\partial\alpha}, \tag{5b}$$

and

$$E_\varphi = -\frac{1}{h_\varphi}\frac{\partial\Phi}{\partial\varphi}, \tag{5c}$$

where $h_\beta=h_\alpha=c/(\cosh\beta-\cos\alpha)$ and $h_\varphi=c\sin\alpha/(\cosh\beta-\cos\alpha)$.

Our goal is then to solve Laplace's equation $\nabla[\varepsilon(\vec{x},\omega)\nabla\Phi]=0$ everywhere, subject to the boundary condition that very far from the two spheres, we have a spatially uniform electric field oriented appropriately. We consider first the case where the external field is parallel to the line between the center of the spheres (z polarized), and then we turn to the case where it is parallel to the xy plane, perpendicular to the axis of symmetry (x polarized).

A. Case where the external field is parallel to the axis of symmetry

In bispherical coordinates, one writes the electrostatic potential in the form

$$\Phi(\beta,\alpha,\varphi) = [2(\cosh\beta - \cos\alpha)]^{1/2}\Psi(\beta,\alpha,\varphi). \tag{6}$$

When the form in Eq. (6) is inserted into Laplace's equation, then the equation for the function Ψ admits separable solutions of the form $\exp[\pm(l+1/2)\beta]P_l^m(\cos\alpha)\exp(im\varphi)$. We can then write the electrostatic potential in the form

$$\begin{aligned}\Phi(\beta,\alpha,\varphi) &= \Phi_{ext}(\beta,\alpha,\varphi) + \delta\Phi(\beta,\alpha,\varphi)\\ &= [2(\cosh\beta - \cos\alpha)]^{1/2}[\Psi_{ext}(\beta,\alpha,\varphi)\\ &\quad + \delta\Psi(\beta,\alpha,\varphi)].\end{aligned} \tag{7}$$

Here, Φ_{ext} is the electrostatic potential for the external laser field, once again assumed spatially uniform in the vicinity of the nanospheres, and $\delta\Phi$ is used to describe the electric fields associated with the response of the nanospheres. For the case under consideration, $\Phi_{ext}=-E_0z$, and one may show that

$$\Psi_{ext} = -\,\mathrm{sgn}(\beta)E_0c\sum_{l=0}^{\infty}(2l+1)\exp\left[-\left(l+\frac{1}{2}\right)|\beta|\right]P_l(\cos\alpha), \tag{8}$$

where $P_l(\cos\alpha)=P_l^0(\cos\alpha)$ is the Legendre polynomial.

We use the separable solutions described above to generate series descriptions of the electrostatic potential in the various spatial domains:

$$\Psi = \sum_{l=0}^{\infty} A_l^{(1)} \exp\left[-\left(l+\frac{1}{2}\right)(\beta-\beta_1)\right] P_l(\cos\alpha) \quad \text{for } \beta > \beta_1, \tag{9a}$$

$$\Psi = \Psi_{ext} + \sum_{l=0}^{\infty} \left\{ A_l^{(2)} \exp\left[\left(l+\frac{1}{2}\right)\beta\right] + B_l^{(2)} \times \exp\left[-\left(l+\frac{1}{2}\right)\beta\right]\right\} P_l(\cos\alpha) \quad \text{for } -\beta_2 < \beta < \beta_1, \tag{9b}$$

and

$$\Psi = \sum_{l=0}^{\infty} A_l^{(3)} \exp\left[\left(l+\frac{1}{2}\right)(\beta+\beta_2)\right] P_l(\cos\alpha) \quad \text{for } \beta < -\beta_2. \tag{9c}$$

The boundary conditions are that the electrostatic potential must be continuous at the surface of each of the two spheres, and then the normal component of $\vec{D}$ is conserved as well. The latter condition is obeyed if one conserves the combination $\varepsilon(\omega)\partial\Phi/\partial\beta$ at the surface of each sphere.

When the forms in Eqs. (9a)–(9c) are submitted to the boundary conditions, we obtain the following relations. First, one can link the sets $\{A_l^{(1)}\}$ and $\{A_l^{(3)}\}$ to the coefficients which appear in Eq. (9b)

$$A_l^{(1)} = -E_0 c(2l+1)\exp\left[-\left(l+\tfrac{1}{2}\right)\beta_1\right] + A_l^{(2)} \exp\left[\left(l+\tfrac{1}{2}\right)\beta_1\right] + B_l^{(2)} \exp\left[-\left(l+\tfrac{1}{2}\right)\beta_1\right], \tag{10a}$$

and

$$A_l^{(3)} = E_0 c(2l+1)\exp\left[-\left(l+\tfrac{1}{2}\right)\beta_2\right] + A_l^{(2)} \exp\left[-\left(l+\tfrac{1}{2}\right)\beta_2\right] + B_l^{(2)} \exp\left[\left(l+\tfrac{1}{2}\right)\beta_2\right]. \tag{10b}$$

We then have a hierarchy of equations from which $\{A_l^{(2)}\}$ and $\{B_l^{(2)}\}$ may be found:

$$l(\varepsilon_1+\varepsilon_0)\exp\left[\left(l-\tfrac{1}{2}\right)\beta_1\right]A_{l-1}^{(2)} + [(\varepsilon_1-\varepsilon_0)\sinh\beta_1 - (\varepsilon_1+\varepsilon_0)\cosh\beta_1(2l+1)]\exp\left[\left(l+\tfrac{1}{2}\right)\beta_1\right]A_l^{(2)} + (l+1)(\varepsilon_1+\varepsilon_0) \times \exp\left[\left(l+\tfrac{3}{2}\right)\beta_1\right]A_{l+1}^{(2)} + l(\varepsilon_1-\varepsilon_0)\exp\left[-\left(l-\tfrac{1}{2}\right)\beta_1\right]B_{l-1}^{(2)} + (\varepsilon_1-\varepsilon_0)[\sinh\beta_1 - \cosh\beta_1(2l+1)]\exp\left[-\left(l+\tfrac{1}{2}\right)\beta_1\right]B_l^{(2)} + (l+1) \times (\varepsilon_1-\varepsilon_0)\exp\left[-\left(l+\tfrac{3}{2}\right)\beta_1\right]B_{l+1}^{(2)} = 2E_0 c(\varepsilon_1-\varepsilon_0)[-le^{\beta_1} + (l+1)e^{-\beta_1}]\exp\left[-\left(l+\tfrac{1}{2}\right)\beta_1\right] \tag{11a}$$

and

$$l(\varepsilon_0-\varepsilon_2)\exp\left[-\left(l-\tfrac{1}{2}\right)\beta_2\right]A_{l-1}^{(2)} + [(\varepsilon_0-\varepsilon_2)[\sinh\beta_2 - \cosh\beta_2(2l+1)]\ \exp\left[-\left(l+\tfrac{1}{2}\right)\beta_2\right]A_l^{(2)} + (l+1)(\varepsilon_0-\varepsilon_2) \times \exp\left[-\left(l+\tfrac{3}{2}\right)\beta 2\right]A_{l+1}^{(2)} - l(\varepsilon_2+\varepsilon_0)\exp\left[\left(l-\tfrac{1}{2}\right)\beta_2\right]B_{l-1}^{(2)} + [(\varepsilon_0-\varepsilon_2)\sinh\beta_2 + (\varepsilon_0+\varepsilon_2)\cosh\beta_2(2l+1)]\exp\left[\left(l+\tfrac{1}{2}\right)\beta_2\right]B_l^{(2)} - (l+1)(\varepsilon_2+\varepsilon_0)\exp\left[\left(l+\tfrac{3}{2}\right)\beta_2\right]B_{l+1}^{(2)} = 2E_0 c(\varepsilon_2-\varepsilon_0)[-le^{\beta_2} + (l+1)e^{-\beta_2}]\exp\left[-\left(l+\tfrac{1}{2}\right)\beta_2\right]. \tag{11b}$$

To obtain the relations in Eqs. (11a) and (11b), one needs to employ recurrence relations among the associated Legendre functions. More details may be found in the discussions give in Ref. 11.

B. Case where the external field is perpendicular to the axis of symmetry

Now, we have $\Phi_{ext} = -E_0 x$, and we find

$$\Psi_{ext} = -2E_0 c \sum_{l=1}^{\infty} \exp\left[-\left(l+\frac{1}{2}\right)|\beta|\right] P_l^1(\cos\alpha)\cos\varphi. \tag{12}$$

We proceed to expand the potential in the various regimes of interest as follows.

For $\beta > \beta_1$,

$$\Psi = \sum_{l=1}^{\infty} A_l^{(1)} \exp\left[-\left(l+\frac{1}{2}\right)(\beta-\beta_1)\right] P_l^1(\cos\alpha)\cos\varphi, \tag{13a}$$

for $-\beta_2 < \beta < \beta_1$,

$$\Psi = \Psi_{ext} + \sum_{l=1}^{\infty} \left\{ A_l^{(2)} \exp\left[\left(l+\frac{1}{2}\right)\beta\right] + B_l^{(2)} \exp\left[-\left(l+\frac{1}{2}\right)\beta\right]\right\} P_l^1(\cos\alpha)\cos\varphi, \tag{13b}$$

and finally for $\beta < -\beta_2$,

$$\Psi = \sum_{l=1}^{\infty} A_l^{(3)} \exp\left[\left(l+\frac{1}{2}\right)(\beta+\beta_2)\right] P_l^1(\cos\alpha)\cos\varphi. \tag{13c}$$

As before, from the boundary conditions, we find the relations

$$A_l^{(1)} = -2E_0 c \exp\left[-\left(l+\tfrac{1}{2}\right)\beta_1\right] + A_l^{(2)} \exp\left[\left(l+\tfrac{1}{2}\right)\beta_1\right] + B_l^{(2)} \exp\left[-\left(l+\tfrac{1}{2}\right)\beta_1\right] \tag{14a}$$

and

$$A_l^{(3)} = -2E_0 c \exp\left[-\left(l+\tfrac{1}{2}\right)\beta_2\right] + A_l^{(2)} \exp\left[-\left(l+\tfrac{1}{2}\right)\beta_2\right] + B_l^{(2)} \exp\left[\left(l+\tfrac{1}{2}\right)\beta_2\right]. \tag{14b}$$

Then, the set of coefficients $\{A_l^{(2)}\}$ and $\{B_l^{(2)}\}$ are found from the hierarchy

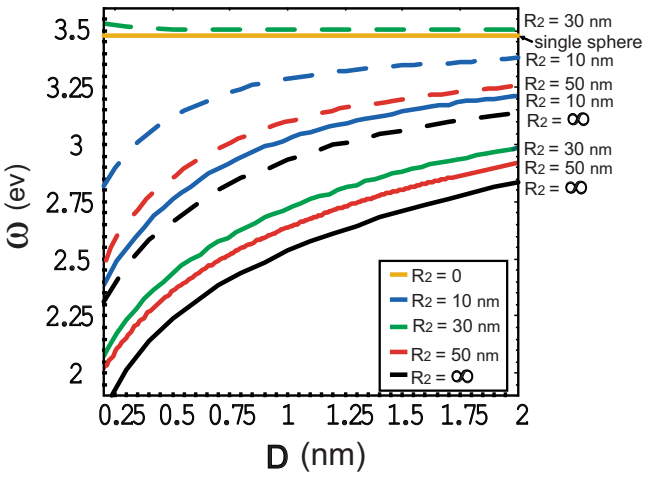

FIG. 2. (Color online) For two Ag spheres, we show the frequency of the lowest lying $m=0$ modes (solid lines) and the lowest lying $m=1$ (dashed lines) modes, as a function of the separation between the poles of the two spheres. One sphere has the radius of 30 nm, and the radius of the second sphere is indicated. The case $R_2=\infty$ refers to a sphere near a plane surface, and we also show the position of the Mie resonance ($l=1$ mode) of the isolated sphere.

$$\begin{aligned}&(l-1)(\varepsilon_1+\varepsilon_0)\exp\left[\left(l-\tfrac{1}{2}\right)\beta_1\right]A_{l-1}^{(2)} + [(\varepsilon_1-\varepsilon_0)\sinh\beta_1 - (\varepsilon_1+\varepsilon_0)\cosh\beta_1(2l+1)]\exp\left[\left(l+\tfrac{1}{2}\right)\beta_1\right]A_l^{(2)} + (l+2)(\varepsilon_1+\varepsilon_0)\\ &\times\exp\left[\left(l+\tfrac{3}{2}\right)\beta_1\right]A_{l+1}^{(2)} + (l-1)(\varepsilon_1-\varepsilon_0)\exp\left[-\left(l-\tfrac{1}{2}\right)\beta_1\right]B_{l-1}^{(2)} + (\varepsilon_1-\varepsilon_0)[\sinh\beta_1 - \cosh\beta_1(2l+1)]\\ &\times\exp\left[-\left(l+\tfrac{1}{2}\right)\beta_1\right]B_l^{(2)} + (l+2)(\varepsilon_1-\varepsilon_0)\exp\left[-\left(l+\tfrac{3}{2}\right)\beta_1\right]B_{l+1}^{(2)} = 4E_0c(\varepsilon_1-\varepsilon_0)\sinh\beta_1\exp\left[-\left(l+\tfrac{1}{2}\right)\beta_1\right]\end{aligned} \tag{15a}$$

and

$$\begin{aligned}&(l-1)(\varepsilon_0-\varepsilon_2)\exp\left[-\left(l-\tfrac{1}{2}\right)\beta_2\right]A_{l-1}^{(2)} + [(\varepsilon_0-\varepsilon_2)[\sinh\beta_2 - \cosh\beta_2(2l+1)]\exp\left[-\left(l+\tfrac{1}{2}\right)\beta_2\right]A_l^{(2)} + (l+2)(\varepsilon_0-\varepsilon_2)\\ &\times\exp\left[-\left(l+\tfrac{3}{2}\right)\beta 2\right]A_{l+1}^{(2)} - (l-1)(\varepsilon_2+\varepsilon_0)\exp\left[\left(l-\tfrac{1}{2}\right)\beta_2\right]B_{l-1}^{(2)} + [(\varepsilon_0-\varepsilon_2)\sinh\beta_2 + (\varepsilon_0+\varepsilon_2)\cosh\beta_2(2l+1)]\\ &\times\exp\left[\left(l+\tfrac{1}{2}\right)\beta_2\right]B_l^{(2)} - (l+2)(\varepsilon_2+\varepsilon_0)\exp\left[\left(l+\tfrac{3}{2}\right)\beta_2\right]B_{l+1}^{(2)} = -4E_0c(\varepsilon_2-\varepsilon_0)\sinh\beta_2\exp\left[-\left(l+\tfrac{1}{2}\right)\beta_2\right].\end{aligned} \tag{15b}$$

The statements above allow us to calculate the electrostatic potential for the two polarizations of the incident driving field of interest. Of course, if one is interested in an applied field in a general direction, one just employs the superposition principle to synthesize expressions for the response of the spheres.

In our discussion in Sec. III, of interest will be the laser-induced force on the pair of spheres. From considerations of translational symmetry, and for the case where the laser field is assumed spatially uniform in the vicinity of the spheres, there can be no net force on the pair. Furthermore, for either polarization, the force must be along the line of symmetry between the spheres, and that on the upper sphere must be equal and opposite in magnitude to the force on the lower sphere. One finds the laser-induced force by integrating the appropriate component of the Maxwell stress tensor over the sphere of interest, evaluating the electric fields just outside the sphere of interest. In bispherical coordinates, the z component of the force may be written as

$$F_z = \varepsilon_0 \int \frac{c^2 \sin\alpha}{(\cosh\beta_1 - \cos\alpha)^2}[(E_\beta E_\beta^* - |E|^2/2)\cos\theta + E_\beta E_\alpha^* \sin\theta]d\alpha d\varphi, \tag{16}$$

where $\theta = \cos^{-1}[(\cos\alpha\cosh\beta_1 - 1)/(\cosh\beta_1 - \cos\alpha)]$.

We conclude with one remark. The statements up to Eqs. (15a) and (15b) can be viewed as either in SI or cgs units. If SI units are employed and we have vacuum outside the spheres, ε_0 is the permittivity of free space, and if cgs units are used, ε_0 is unity. The form in Eqs. (15a) and (15b) is valid in only SI units, as written. We turn next to a discussion of the numerical results we have obtained, within the above framework.

III. RESULTS AND DISCUSSION

In this section, we present a series of calculations which explore issues related to the collective mode spectrum of two dissimilar metallic nanospheres and their influence of the response characteristics of the system. We find adequate convergence if the hierarchy of equations derived above is terminated at the value $l=l_{max}\sim 40$. It will be apparent from the results we present that the dipole approximation sometimes used to model interactions between two nearby spheres is quite inadequate. The dipole approximation is valid only if the separation between nearby spheres is large compared to their radius, as noted above. When they are in close proximity to each other, high order multipoles enter in an essential manner.

In Fig. 2, to illustrate the influence of size mismatch on the nature of the collective modes of a system of two spheres, we show the frequency of the lowest lying collective plasmon modes of the pair as a function of the separation between the poles of the two spheres. Both spheres are taken to be Ag, and the radius of one is fixed at 30 nm while that of the second is varied. The solid lines show the behavior of the low lying $m=0$ modes, while the dashed lines are the lowest frequency $m=1$ modes. These curves have been constructed from the resonant peaks in enhanced field calculations such as those in Fig. 3. The $m=0$ resonances are excited by an external field parallel to the line between the centers of the spheres, and the $m=1$ modes are excited when the field is perpendicular to this line, as we have seen in Sec. II.

We see that as the radius R_2 increases, the frequency of the low lying modes decreases in a monotonic manner. The Mie resonance of the isolated Ag sphere, which is the lowest lying collective plasmon mode of the isolated sphere (this is the $l=1$ mode), is shifted down into the visible range of frequencies from the near ultraviolet by virtue of the interaction between the spheres.

In Fig. 3, for two spheres separated by 2 nm, we show the frequency variation of the enhanced fields that are realized for three cases. All calculations are for two Ag spheres; one (sphere 1) has radius of 30 nm and the second (sphere 2) with radius R_2 indicated. We show the value of $r=|\vec{E}/E_0|^2$, with E_0 the incident field. In Fig. 3(a), we show results for the case where the incident field is parallel to the line between the sphere centers, and in Fig. 3(b), the incident field is perpendicular to the line between centers. The field $\vec{E}$ is calculated at the position on the 30 nm sphere where the field enhancement is largest. In Fig. 3(a), as we shall see, the field is largest at the pole of sphere 1 that is closest to sphere 2. In Fig. 3(b), the point of maximal field enhancement is removed a bit from this pole. Notice that, on the whole, the maximum values of the enhanced fields are realized for the case where sphere 2 has the radius of 50 nm. Below the first collective mode peak just above 3 eV, we see that the enhanced fields are larger than for two identical spheres for the case where sphere 2 has radius 50 nm. In Fig. 3(a), at the highest frequency collective mode resonance, above 3.4 eV, the ratio r is about an order of magnitude larger when R_2 is 50 nm than for the case where the two spheres are identical. If we have

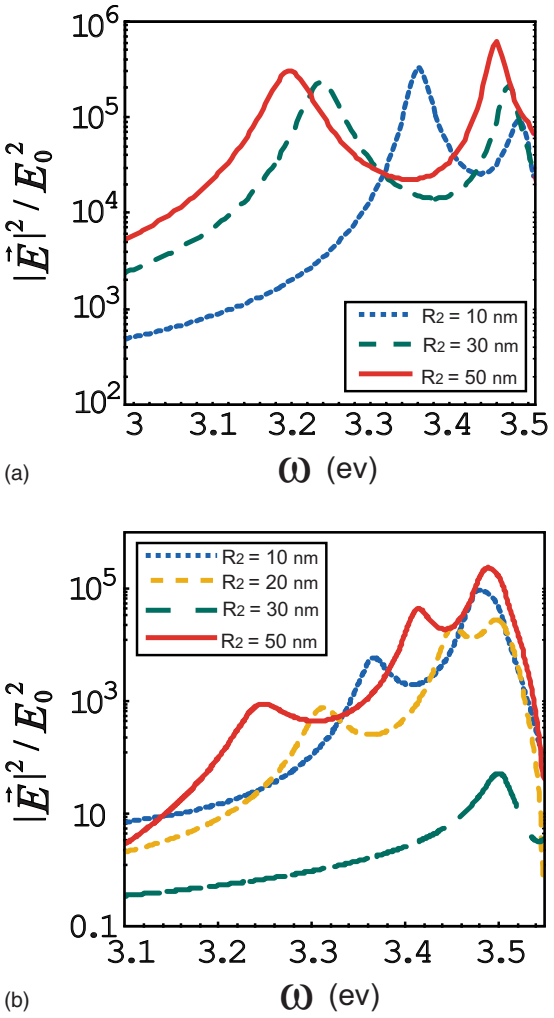

FIG. 3. (Color online) The frequency dependence of the enhanced fields realized for two Ag spheres separated by 2 nm. The radius of one sphere is 30 nm, and the second assumes the value indicated. The fields are calculated at the point on the 30 nm sphere where the enhanced field assumes it maximum value. See the discussion in the text for more details. In (a), we have the external field parallel to the line of sphere centers and in (b) perpendicular to this line.

SERS in mind, the Raman signal scales as r^2. Thus, if maximal enhancement is realized for a molecule located in the gap between the two spheres, the SERS signal would be roughly 100 times stronger when $R_1=30$ nm and $R_2=50$ nm, compared to the case of two identical spheres with $R_1=R_2=30$ nm. Clearly, the largest field enhancements are obtained for the case where the applied field is parallel to the line between the centers of the spheres. Of course, in both Figs. 3(a) and 3(b), the peaks are produced by excitation of collective plasmon resonances.

One interesting feature of Fig. 3(b) is the following. When the two spheres have identical radii, we have a selection rule operative regarding which collective modes can be excited by a laser field perpendicular to the line between the sphere centers, and also for the case where the exciting field is parallel to the line between the sphere centers. First, for any

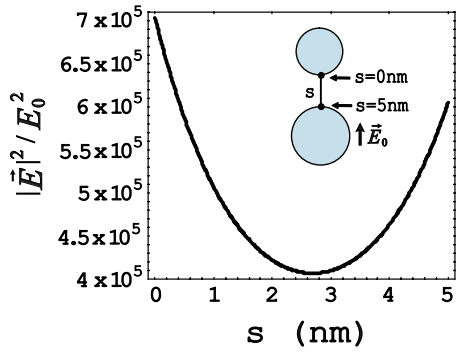

FIG. 4. (Color online) For a sphere whose radius is 30 nm and a sphere whose radius is 50 nm, we show the enhanced electric field as a function of distance between the two poles of the sphere. The exciting field is 3.46 eV, on resonance with the feature that provides the largest enhancement of the field, and the two poles are separated by 5 nm. The exciting field is parallel to the line between the centers of the two spheres.

value of the azimuthal quantum number m, we have collective modes which lie below the Mie resonance of the isolated sphere and modes which lie above. If m is even (odd), the electrostatic potential associated with the lower branches is odd (even) under reflection through the line of centers, and for the upper branches, the potential is even (odd) under reflection through this plane. If the laser field is perpendicular to the line of centers, then we have seen from Sec. II that it is the $m=1$ modes that are excited by the laser field, and the modes which have the appropriate symmetry are those which lie above the Mie resonance of the isolated sphere. Thus, in Fig. 3(b), we see no resonances in the enhanced field below 3.5 eV for the case where $R_1=R_2=30$ nm. However, when the spheres are dissimilar, the selection rule just discussed breaks down, and in Fig. 3(b), we see a sequence of resonant peaks in the region 3.1–3.5 eV. These have origin in excitation of the modes which lie below the Mie resonance, and the structures appear by virtue of the breakdown of the selection rule appropriate to identical spheres. A consequence of the breakdown of the selection rule is that much larger enhanced fields can be realized in the spectral region illustrated when the spheres are dissimilar, compared to the case of identical spheres. The effect on SERS of the breakdown of the selection rule is very dramatic if one appreciates that the SERS intensity scales as $|\vec{E}/E_0|^4$. A comparison between Figs. 3(a) and 3(b) shows that for perpendicular excitation, one can realize field enhancements quite comparable to those found when the exciting field is parallel to the axis of symmetry.

We comment next on the spatial distribution of the field enhancement. In Fig. 4, for two spheres, one with radius of 30 nm and the second with 50 nm, we show the variation of the ratio r defined above as one moves along the line of centers between the two spheres, from the "south pole" of the 30 nm sphere where the enhancement is maximum to the "north pole" of the larger sphere. The calculation assumes that the separation between the two poles is 5 nm and that the exciting field is parallel to the line between the two centers. The photon energy has been taken to be 3.46 eV, where

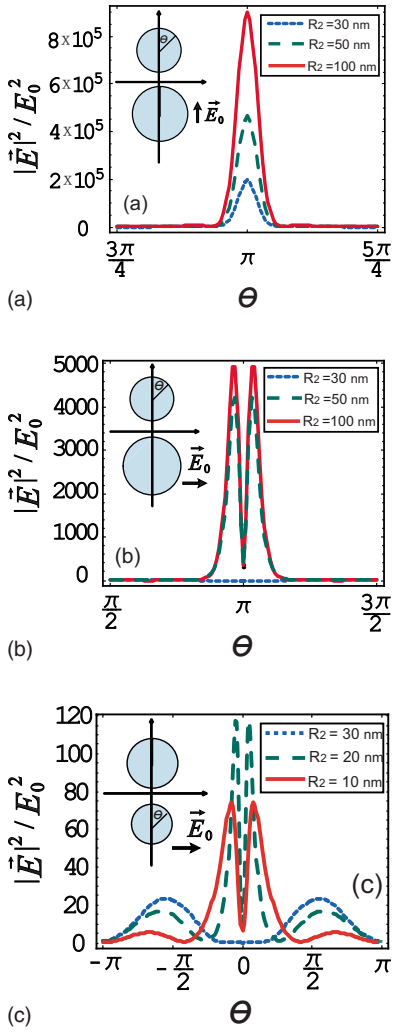

FIG. 5. (Color online) The angular dependence of the enhanced field near the pole of the 30 nm sphere where maximum field enhancement is realized. Both spheres are Ag, the separation between their poles is 1 nm, and the photon frequency is 3.1 eV. In (a), the exciting field is parallel to the axis between the centers of the two spheres, and in (b) and (c), the field is perpendicular to this axis.

one realizes the largest resonant enhancement. One sees that the field is enhanced quite strongly along the entire line.

In Fig. 5, we illustrate the angular variation of the field intensity near the pole of the sphere whose radius is 30 nm. In Fig. 5(a), the exciting field is parallel to the line between the centers of the two spheres, and in Figs. 5(b) and 5(c), the exciting field is perpendicular to the line between centers. The distance between the two spheres is 1 nm, and the exciting field consists of photons with the energy of 3.1 eV. We see that in the first case, the maximum value of the field is right at the pole, whereas when the exciting field is perpendicular to the centers, there is actually a sharp dip in intensity at the pole, and the maximum field is offset a bit from the pole. Quite clearly, a dipole picture is unable to describe fields with this character, since high order multipoles must be included to describe such highly localized fields.

So far, our discussion has focused it attention on pairs of Ag spheres and the influence of differences in radii. It is

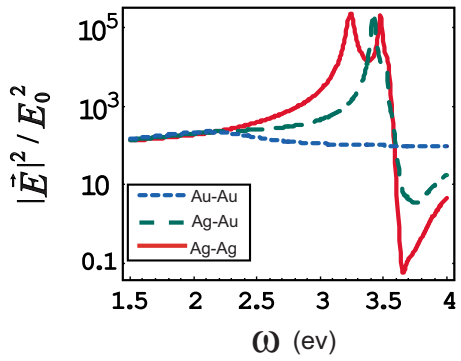

FIG. 6. (Color online) The maximum enhanced fields realized for two spheres whose radius is 30 nm. In one case, we have a pair of Ag spheres; in a second one, we have one Ag sphere and one Au sphere; and in the third, we have two Au spheres. The poles of the spheres are separated by 5 nm, and the exciting field is parallel to the line of centers between the two spheres.

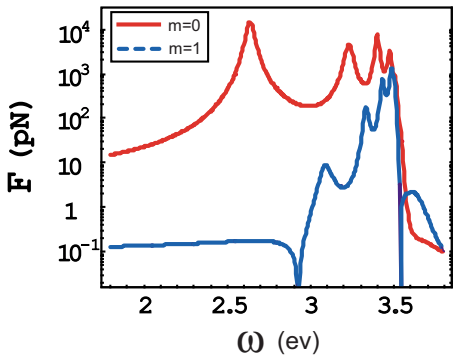

FIG. 7. (Color online) The dependence on photon frequency of the magnitude of the laser-induced force between two Ag spheres whose poles are separated by $d=1$ nm. The spheres have radii of 30 and 50 nm, respectively. The solid curve is the force induced by an exciting field parallel to the line between the centers of the spheres, and the dotted curve is for an exciting field perpendicular to the line between the centers of the spheres. The incident laser power has been taken to be 10 mW/μm^2.

interesting also to examine the case where the spheres are fabricated from two different materials. In Fig. 6, we compare the maximum enhanced fields realized when one sphere is fabricated from Au and when both spheres are fabricated from Au. Both spheres have identical radii, 30 nm, and the separation between the two spheres is 5 nm in these calculations. The exciting field is parallel to the axis of symmetry for these calculations. When we compare the case where one sphere is fabricated from Au to the case where both spheres are Ag, we see that the maximum enhanced field realized is roughly the same. However, the low frequency structure in the doublet one sees for the Ag/Ag case is absent. The Mie resonance of an isolated Au sphere lies much lower in frequency than that for Ag, in the vicinity of 2.2 eV. Because of the higher intrinsic dissipation in Au, it is quite a broad structure, with the consequence that the enhanced fields one can realize are much smaller. In Fig. 6, one can appreciate this; there is quite a broad structure for the Au pair near 2 eV, and the field enhancements realized are quite small compared to Ag pairs.

The calculations in Fig. 6 extend to higher frequencies than our earlier results. We note the striking minimum just above 3.5 eV for the two Ag sphere case. When the spheres are driven by a frequency above the collective resonance frequencies, the field generated by charge motions in the spheres is roughly 180° out of phase with the driving field, thus producing the minimum. As we move to still higher frequencies, we enter the regime of interband transitions and the physical picture is not so simple.

We now turn to our calculations of the laser-induced force between the two spheres. We begin by referring the reader to the discussion in our previous publication.[14] In Fig. 2 of Ref. 14, we show the variation with distance between the poles the laser-induced force between two identical Ag spheres and between one Ag sphere with radius 30 nm and a second Ag sphere with radius 60 nm. This is done for two photon energies, and the figure refers to the case where the exciting field is parallel to the line between the centers of the spheres. It is the case that for two identical Ag spheres, the force is very much smaller by 2 or 3 orders of magnitude for photon energies below ~3.5 eV, if the exciting field is applied perpendicular to the line of centers. This is because there are no collective modes below the isolated sphere Mie resonance whose symmetry allows them to be excited by the exciting field.

However, if one considers two spheres of dissimilar radius, the breakdown of the selection rule as discussed above allows a laser field applied perpendicular to the line of centers to excite the low lying collective modes, as we have seen. A consequence is that for this case, one can realize laser-induced forces comparable in strength in perpendicular excitation to those realized in parallel excitation. We illustrate this in Fig. 7.

In the examples discussed in Ref. 14, and for the calculations displayed in Fig. 7 of the present paper, the laser-induced force is attractive. It is interesting that for the case of excitation with field perpendicular to the line between the centers of the sphere, it is possible to realize repulsive forces between the spheres, under suitable circumstances. The force is attractive for the $m=1$ curve in Fig. 7, between the zeros near 2.9 and 3.55 eV, and is repulsive in the range of rest frequencies. We show another example of this behavior in Fig. 8. The dotted curve shows, for perpendicular excitation, the magnitude of the laser-induced force between two Ag spheres as a function of the distance between their poles. One sphere has radius of 30 nm and the second 50 nm, and the photon energy is taken to be 3.1 eV. We see collective mode resonances with origin in the breakdown of the selection rule for identical spheres. Notice, in the dotted curve, the zero near $d=2$ nm. Below this zero, the laser-induced force is attractive, while above it the force between the spheres is repulsive. The solid line in the upper right portion of the figure is the strength of the van der Waals attraction between the spheres, calculated as discussed in Ref. 14. Unfortunately, in the interesting regime where the laser-induced force is repulsive, its magnitude is quite small compared to the van der Waals attractive force. Of course, the laser-induced force scales linearly with laser power, so with a

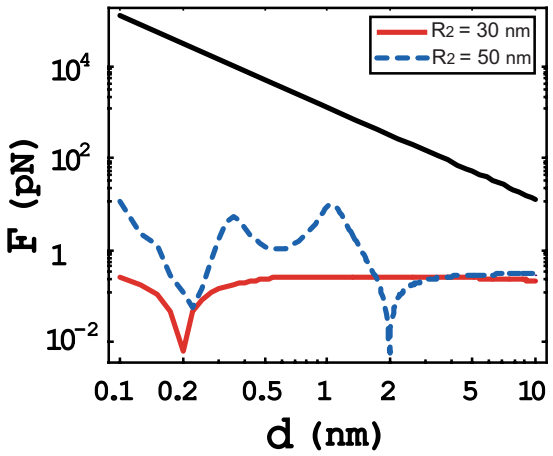

FIG. 8. (Color online) Calculations of the dependence of the magnitude of the laser-induced force between two Ag spheres for the case where the exciting field is applied perpendicular to the line between their centers. One sphere has radius of 30 nm, and the second the radius indicated. The laser power has been taken to be 10 mW/μm^2, and the photon energy is 3.1 eV. For the case of dissimilar spheres, the force is repulsive rather than attractive for separations greater than 2 nm, while for the case of the two identical spheres, it is repulsive above the separation of 0.2 nm.

suitable increase of laser power over the value used in these calculations (10 mW/μm^2), it may be possible to boost the repulsive force up to the point where it overwhelms the van der Waals attraction. With cw excitation, this would lead to heating and various complications. However, through use of intense short pulses, it seems reasonable to us that one may boost the force to the point where it exceeds the van der Waals attraction. The solid curve in Fig. 8 is a calculation of the magnitude of the force for two identical Ag spheres whose radii are 30 nm. The collective mode resonances are absent, but now the force is repulsive for all pole separations which exceed 0.2 nm.

We conclude this section with calculations of the laser-induced force between a Ag sphere and a Au sphere placed nearby. We saw earlier that even though Au is quite lossy, one can realized enhanced fields for the Ag/Au combination comparable to those realized for the Ag/Ag case. This is the case as well for the laser-induced force. We illustrate this in Fig. 9 for the case of a laser field applied parallel to the line of centers between the spheres.

IV. CONCLUDING REMARKS

In this paper, we have presented a series of calculations of enhanced fields and laser-induced forces realized in the vicinity of two metallic spheres placed in close proximity to each other. The emphasis is on the case where the two spheres are dissimilar, either with different radii or composed of different materials.

If the two spheres are identical, then the enhanced fields and the magnitude of the laser-induced force between them are much larger for laser fields applied parallel to the line between the centers than for the case when the field is perpendicular to the line between the centers. This remark, for the ideal material Ag, applies to frequencies in the visible range, which lie below the Mie resonance of the isolated Ag sphere. The reason for this is that symmetry forbids excitation of the relevant collective plasmon modes, for the case of perpendicular excitation. For dissimilar spheres, our calculations show that the selection rule breaks down quite dramatically, and we then find enhanced fields and laser-induced forces of comparable magnitude can be realized for both geometries.

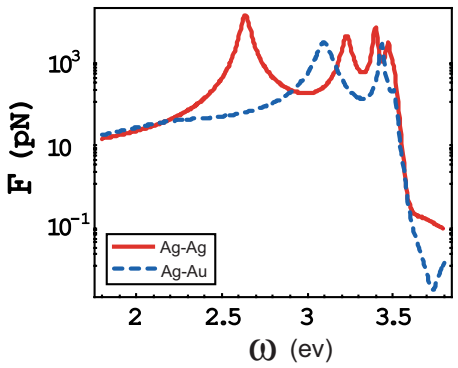

FIG. 9. (Color online) We provide a comparison between the laser-induced force between two Ag spheres and between a Ag sphere and a Au sphere. One sphere has radius of 30 nm, and the second 50 nm; the Au sphere is the larger in the Ag/Au example. The exciting field is applied parallel to the line between the centers, the separation between the poles of the two spheres is 1 nm, and the laser power has been taken to be 10 mW/μm^2.

The calculations here and those presented in Ref. 14 suggest that for modest laser powers, exploitation of the collective plasmon resonances can result in laser-induced forces in excess of the van der Waals force. It is the case as well that for perpendicular excitation, the laser-induced force can be repulsive for suitable geometries and frequency regimes. These results, in our mind, are of potential interest in regard to laser manipulation of nanoparticle structures. The use of pulsed laser sources will allow powers greatly in excess of those utilized in the calculations reported here, so one has the possibility of entering the regime where the total force between two spheres (van der Waals+laser-induced force) is, in fact, repulsive.

It would be of fundamental interest also to see measurements of the laser-induced force between two spheres. This is, in principle, a physically accessible quantity which may be used as a test of calculations such as ours. If laser-induced forces comparable to those calculated are indeed realized, then one can infer that the very large enhanced fields calculated are realized as well, near the two closest poles of the spheres. Such a measurement would allow one to make direct inferences regarding the strength of the enhanced fields realized with real materials. We can envision measurement of the laser-induced force between a sphere attached to an atomic force microscope tip and a suitable plane surface. Quite clearly, the optimum material is Ag for both the sphere and the substrate.

While our discussion is confined to the case of a pair of nanospheres, it is also of great interest to explore related

issues for linear arrays, finite and infinite in nature, and also for other arrangements of nanospheres. Once again, we direct the reader to the formalism developed and implemented in Ref. 10. This is a exact real space formulation, within the electrostatic approximation employed here, of the response of arrays of spheres. This method can be applied to a diverse range of problems in this area.

ACKNOWLEDGMENTS

During the course of this research, we have enjoyed stimulating conversations with A. Apkarian, J. C. Hemminger, and Wilson Ho. This research was supported by the U.S. Department of Energy, through Grant No. DE-FG03-84ER-45083.

*pingc@uci.edu

†dlmills@uci.edu

[1] M. Fleischmann, P. J. Hendra, and A. J. McQuillan, Chem. Phys. Lett. **26**, 163 (1974); M. Fleischmann, P. J. Hendra, A. J. Mcquillan, R. L. Paul, and E. S. Reid, J. Raman Spectrosc. **4**, 269 (1976).

[2] For a collection of papers which discuss the early phase of SERS studies, see *Surface Enhanced Raman Scattering*, edited by Richard K. Chang and Thomas E. Furtak (Plenum, New York, 1982).

[3] M. Udagawa, C. C. Chou, J. C. Hemminger, and S. Ushioda, Phys. Rev. B **23**, 6843 (1981).

[4] D. L. Mills and M. Weber, Phys. Rev. B **26**, 1075 (1982).

[5] J. C. Tsang, J. R. Kirtlet, and T. N. Theis, Solid State Commun. **35**, 667 (1981).

[6] Shuming Nie and Steven R. Emory, Science **275**, 1102 (1997).

[7] Hiroharu Tamarua, Hitoshi Kuwata, Hideki T. Miyazaki, and Kenjiro Miyano, Appl. Phys. Lett. **80**, 1826 (2002).

[8] W. Rechberger, A. Hohenau, A. Leitner, J. R. Krenn, B. Lamprecht, and F. R. Aussenegg, Opt. Commun. **220**, 137 (2003).

[9] Stefan A. Maier, Mark L. Brongersma, Pieter G. Kik, and Harry A. Atwater, Phys. Rev. B **65**, 193408 (2002).

[10] Rodrigo Arias and D. L. Mills, Phys. Rev. B **68**, 245420 (2003).

[11] D. L. Mills, Phys. Rev. B **65**, 125419 (2002); Shiwei Wu and D. L. Mills, *ibid.* **65**, 205420 (2002).

[12] S. W. Wu, N. Ogawa, and W. Ho, Science **312**, 1362 (2006).

[13] Juris Prikulus, Fredrik Svedberg, and Mikael Kall, Nano Lett. **4**, 115 (2004).

[14] Ping Chu and D. L. Mills, Phys. Rev. Lett. **99**, 127401 (2007). An erratum to this paper has been submitted to Physical Review Letters. The erratum corrects modest quantitative errors with origin in a small error in the code used to generate these results.

[15] P. K. Aravind, A. Nitzan, and H. Metiu, Surf. Sci. **110**, 189 (1981).